Identification and Measurement of Positive and Negative Topological Charges of LG Beams for Medical Care

Jianjun Guo[1,2,3,†], Shahbaz Gul Hassan[1,2,3,†], Lijun Lin[1,2,3], Tonglai Liu[1,2,3], Liang Cao[1,2,3], Dachun Feng[1,2,3], Shuangyin Liu[1,2,3,4,*] and Longqin Xu[1,2,3,*]

[1] Guangzhou Key Laboratory of Agricultural Products Quality & Safety Traceability Information Technology, Zhongkai University of Agriculture and Engineering, Guangzhou 510225, China
[2] College of Information Science and Technology, Zhongkai University of Agriculture and Engineering, Guangzhou, 510225, China
[3] Academy of Intelligent Agricultural Engineering Innovations, Zhongkai University of Agriculture and Engineering, Guangzhou 510225, China
[4] College of Mechanical and Electric Engineerings Shihezi University, Shihezi, 832000, China
[†] Contributed equally to this work.
[*] Corresponding author, contributed equally.
E-mail address: shuangyinliu@zhku.edu.cn, mhasan387@zhku.edu.cn

Abstract. A medical care system's security, high-capacity information transfer, and communication are all dependent on OAM-based quantum key distribution, namely on the measurement of OAM's topological charges (TCs). The intensity patterns of interference between the vortex beam and its conjugate beam are analyzed to detect and evaluate positive and negative TCs of Laguerre-Gaussian (LG) vortex beams in a novel manner. An upgraded Mach–Zehnder (M-Z) interferometer is used to establish the order of positive, negative, integer, and half-integer TCs. Deciphering the order of integer TCs and half-integer TCs may be accomplished by measuring the interference bright petals as well as half of the total numbers of bright petals. The integer and half-integer TCs (VPP) may be modulated by the use of light path rotational with a vortex stage plate. Using the interferometer as mentioned earlier, the positive and negative of integer and half-integer TCs are acquired. Quantitatively, the order and sign of integer and half-integer TCs are measured in this manner. And this method is straightforward and less susceptible to the influence of parasitic interference. This can provide comprehensive security protection for the medical monitoring system, better reduce medical risks and protect patient privacy.

1. Introduction

With the development of society, people gradually improve the quality-of-life requirements, more and more attention to medical care services. Due to the promotion of information technology and network technology, making up for the shortage of many traditional medical services [1-9]. Medical care system is a kind of physiological and biochemical parameters of patients with a continuous, long time, automatic, real-time monitoring, data analysis and processing after implementation class automatic alarm, automatic recording some of the more the combination of medical instruments, electronic technology, computer technology, communication technology, biological detection technology and the

combination of the relevant technology of modern medicine [10-15]. The functional module diagram of the medical care system is shown in figure 1. Because it can be used for real-time analysis, display and long-term recording of the concerned parameters, and has certain comprehensive judgment ability for the results, it can timely remind and help the medical staff to make appropriate judgment and treatment of the patient's condition changes, greatly reducing the workload of medical staff. The medical care system consists of three major parts: body domain network, local gateway and remote monitoring centre. Its architecture diagram is shown in figure 2.

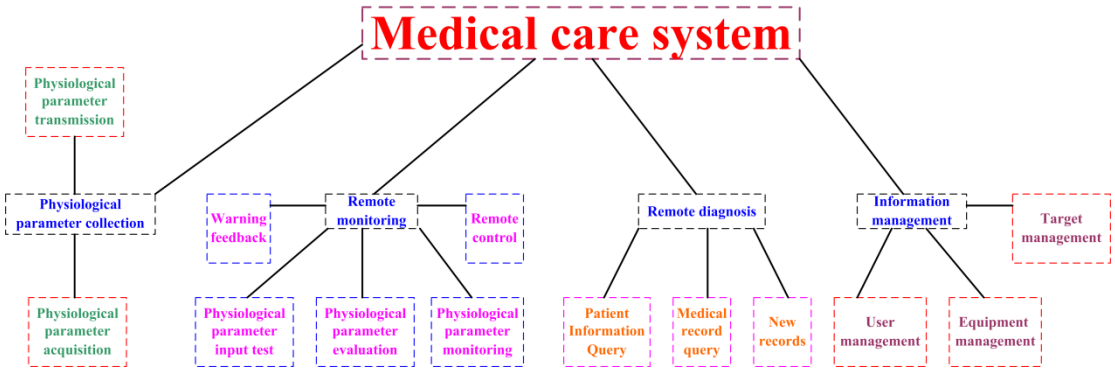

Figure 1. The functional module diagram of the medical care system.

Medical monitoring systems need secure data. Quantum key distribution based on orbital angular momentum (OAM) provides excellent security, big capacity transfer of information and communication. Measuring of OAM topological charges (TCs) is crucial. High security, data transfer encryption, secure transmission via network connection. Various network people are sharing a same set of GPRS channels, but only when a user wants to transmit or receive data. Identification and measurement of positive and negative topological charges of LG beams can provide comprehensive security protection for the medical monitoring system, reduce medical risks and protect patients' privacy.

A rising amount of attention has been focused on the so-called optical vortex beam, which has a clearly defined OAM [16]. The phase factor $\exp(il\theta)$, azimuthal coordinate θ, l and time constant (TC) all go hand in hand when describing an optical vortex. The TC accepts positive (negative) values in addition to integers, zeros, and fractions. The OAM of vortex beams may therefore be used for a variety of important purposes, including optical communication [17-20], quantum storage [21], remote sensing [22], micro-particle manipulation [23-25], integrated waveguide [26-28], internet of things [29-32], and so on. As a result, it is crucial to measure TCs precisely using both the order and the sign There have been many approaches to measuring TCs up to this point, where the order and the sign are important considerations [33-42]. Adjusting TCs with a vortex phase plate (VPP) [43]. After an odd number of reflections, TC of vortex beam is reversed [44]. For measuring TCs, on account of their simplicity, diffraction methods have been generally used in recent years [34, 35]. After an annular aperture, it is possible to quantify the TCs of an optical vortex beam by analysing its diffraction intensity pattern. l=9 [34]. TCs are calculated with respect to $l=14$ to use a tilted convex lens [35]. Vortex beam and conjugate beam interference patterns increased TC $l=60$ [37]. Which used a modified Mach–Zehnder (M-Z) interferometer [39], TC has reached $l=90$. Through the use of two improved m-z interferometers in 2016, our research group has been able to measure not only TC of positive 90 OAM, but also TC of negative 90 OAM [40]. That is to say, the sign of TC of Laguerre-Gaussian (LG) vortex beams can be determined. In the measuring system, however, certain optical components, such as the dove prism (DP), produce parasitic interference. Additionally, the mechanism is fairly complex.

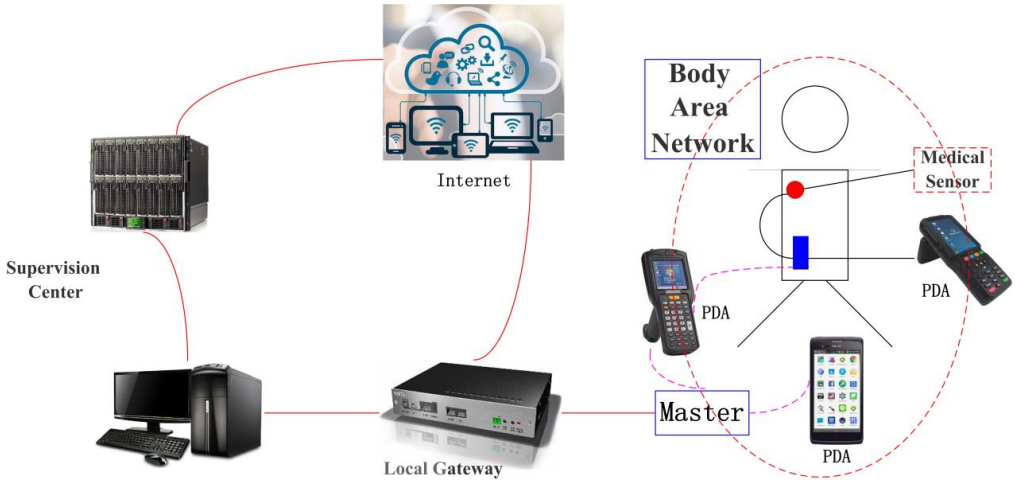

Figure 2. The architecture diagram of the medical care system.

LG vortex beam TCs may now be measured using an enhanced M-Z interferometer with five mirrors, a rectangular light path circulation (VPP), and an enhanced M-Z interferometer with five mirrors as a result of this research. The formula may be used to calculate the order of integer and half-integer TCs by calculating the frequency of interference bright petals within LG beam or its conjugate beam. Another way to determine the sign of integer and half-integer TCs is to circulate a rectangular light channel with a VPP and then use the previously stated interferometer. In contrast to earlier approaches, our presented method can not only measure the order of TCs, but also can measure the positive and negative of TCs. To prepare the conjugate vortex beam, we use a few of simple mirrors instead of the expensive DP. Because of no DP in our system, it is straightforward and less susceptible to the influence of the parasitic interference. This can provide comprehensive security protection for medical care system, high capacity information transmission, reduce medical risks and protect patient privacy.

2. Theoretical Analysis

An opaque phase plate with a predetermined index of refraction separates the vortex phase plane and planar surface structures. The angular azimuth of the VPP is related to its thickness. The optical path difference and degree of phase shift of the transmission beam are both affected by the vortex surface of the VPP. Figure 3 illustrates the output vortex beam's phase and intensity distributions as a Gaussian input beam passes through the VPP. The TC rises by one magnitude whenever the input vortex beam travels through to the VPP at all during the rectangular frequency increases cycle [43].

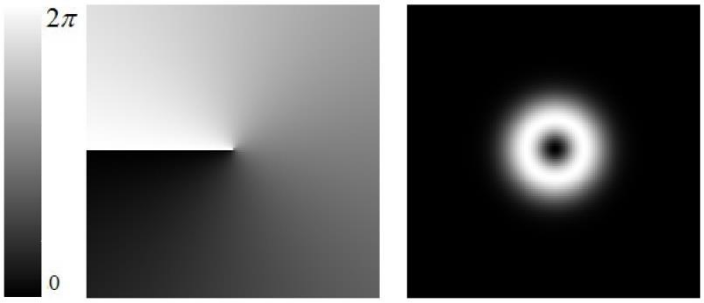

Figure 3. Phase distribution and intensity distribution of the output vortex beam through the VPP.

When the control signal of grating crystal control device (GCCD) is setting, incident vortex beam is reflected by the GCCD, namely, it doesn't go into the rectangular circular light path. When the

control signal of the GCCD is resetting, incident vortex beam enters and gets out of the rectangular circular light path by transmission of the GCCD.

In cylindrical dimensions, the condensed LG vortex beam equation [37] is:

$$E_1(r,\theta)=\left(\frac{r}{w_0}\right)^{|l|}\times\exp\left(-\frac{r^2}{w_0^2}\right)\times\exp(il\theta), \tag{1}$$

w_0 is the LG vortex beam's waist width, and l is its TC.

$$E_2(r,\theta)=\left(\frac{r}{w_0}\right)^{|l|}\times\exp\left(-\frac{r^2}{w_0^2}\right)\times\exp(-il\theta), \tag{2}$$

As a result, the arrangement of interference frequency in between LG vortex beam but also its conjugate generates $I(r,\theta)=\left|E_1(r,\theta)+E_2(r,\theta)\right|^2$

$$=\left|\left(\frac{r}{w_0}\right)^{|l|}\times\exp\left(-\frac{r^2}{w_0^2}\right)\times\exp(il\theta)+\left(\frac{r}{w_0}\right)^{|l|}\times\exp\left(-\frac{r^2}{w_0^2}\right)\times\exp(-il\theta)\right|^2$$

$$=2\left(\frac{r}{w_0}\right)^{2|l|}\times\exp\left(-\frac{2r^2}{w_0^2}\right)\times\left[1+\cos(2l\theta)\right], \tag{3}$$

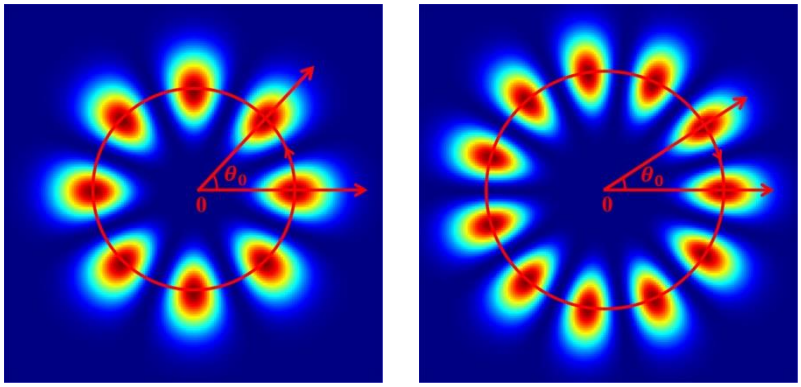

(a) (b)

Figure 4. (The difference in height between two neighboring petals $\theta_0=\pi/l$, Vortex beam and so its conjugate beam interfering frequency patterns (a). (b) the patterns of interference between both the vortex beam $l=+4$ and thus its conjugate beam $l=-5.5$.

The interference fringe pattern exhibits a circular symmetry distribution modified by cosine. Using the first-order partial derivatives of Equation (3) with respects to θ, the angle among two successive fringes is computed.

$$\frac{\partial I(r,\theta)}{\partial\theta}=-4l\left(\frac{r}{w_0}\right)^{2|l|}\exp\left(-\frac{2r^2}{w_0^2}\right)\sin(2l\theta), \tag{4}$$

Furthermore, Eq. (3) with regard to θ is given in terms of second-order partial derivatives

$$\frac{\partial^2 I(r,\theta)}{\partial\theta^2} = -8l^2\left(\frac{r}{w_0}\right)^{2|l|}\exp\left(-\frac{2r^2}{w_0^2}\right)\cos(2l\theta), \tag{5}$$

If $\frac{\partial I(r,\theta)}{\partial\theta} = 0$ and $\frac{\partial^2 I(r,\theta)}{\partial\theta^2} < 0$, For the sake of simplicity, we may omit $\theta = \pi/l$ The angle created by two neighbouring petals, represented by $\theta_0 = \pi/l$ and shown visually in Figure 4, is then determined.

A simulation of reflected signal in between vortex beam and the at symbol and its conjugate beam produced these findings, which are shown in the following figure: (a). Using the vortex beam with and its conjugate beam as an interference source, we were able to simulate the interference patterns seen in figure 4. (b). As a consequence, the relationship between the TC values and the number of petals n may be described using a formula. The sequence of numerical and half-integer TCs may be verified by tallying the interference luminous petals, when no indication can be detected. Despite the fact that the sign itself cannot be read, this is nonetheless the case. The subsequent experiment, on the other hand, will be capable of determining the sign of TCs that are either integers or half-integers.

3. Experimental Setup

Fig. 5 depicts the experimental setup, which consists of a rectangular light channel circulation with a VPP (RPC Photonics VPP-1c) and an enhanced equi-arm M-Z interferometer with five mirrors. These components are combined to form the interferometer. The He-Ne laser has a wavelength of 632.8 nm, and a beam expander (BE, 10) collimates and expands the Gaussian beam that comes from the laser. The light source is a 632.8 nm laser. The spatial light modulator (SLM, PLUTO-NIR-010-A) is controlled by a computer to create the LG vortex beam. In order to produce the LG vortex beam, a computer analyses the spatial light modulator (PLUTO-NIR-010-A). The SLM created this beam. LG vortex and forked grating are used in this modulator, as indicated in Equation (1). The creation of the LG vortex beam starts once the SLM has been illuminated.

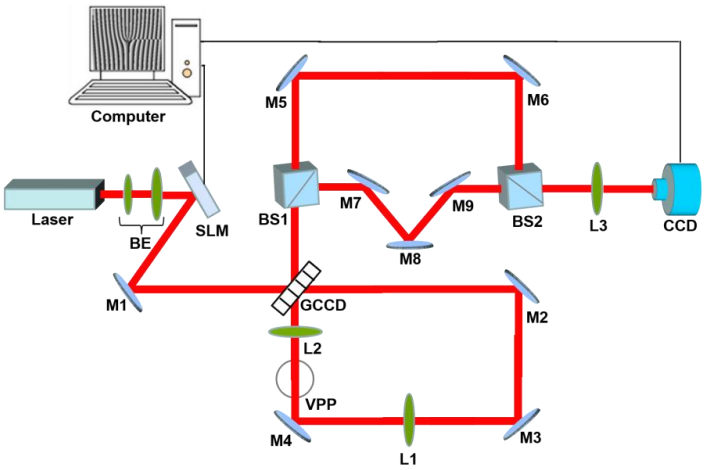

Figure 5. Method for determining whether or not an LG vortex beam has ordered and signed TCs. BS1, BS2: Beam Splitters; M1-M9: Mirrors; L1-L3: Lenses. BE: Beam Expander. GCCD: Grating Crystal Control Device. VPP: Vortex Phase Plate. SLM: Spatial Light Modulator.

During the establishment of the GCCD control signal, the LG vortex beam that's been deflected by M1 and GCCD is separated into two distinct vortex beams through the use of a beam splitter (BS1). Before BS1, the LG vortex beam encounters a twofold reflection; as a consequence, the sign of the LG vortex beam's TC does not change. Three mirrors make up the bottom arm of the M–Z interferometer,

which contains one vortex beam. This beam is then reflected four times by the beam splitters BS1, M7, M8, and M9. Therefore, there is no change in the sign of the TC of a single vortex beam, which is specified by equation (1). The second is positioned on the right forearm of the M–Z interferometer, one that is split into two mirrors thus reflects light three times due to M5, M6, and BS2. As a result, the sign of TC of the other one is the opposite, which is established by the equation (2). Equi-arm functionality is achieved inside the M–Z interferometer by use of these five mirrors. Charge-coupled devices are ultimately employed to record and store diffraction pattern between both the LG vortex beam as well as its conjugate beam on the a computer (CCD). L3, which has a focal length of 150 millimetres, is employed prior to CCD (DH-SV2001GC) to minimize the growth of the vortex region. The LG vortex light and its complementary beam are simulated in order to identify their diffraction gratings. Eq. (3). T Fig. 6-9 shows simulated and numerical findings with l=+2 , +3 , −2.5 and −3.5 . The probable patterns of TCs with l=+2 , +3 , −2.5 and −3.5 correspondingly are shown on the left side of Fig. 6-9. And Fig. 6-9(right) are the experimental results of Fig. 6-9(left). Both the theoretical conclusions and the experimental data are consistent with one another. Each peak in the interference figures can be seen in a bright petal, and also the inclination between any two consecutive edges is denoted by $\theta_0 = \pi/l$. Like a consequence, we calculate the relationship here between TC indices l and the frequency of petals with $\theta_0 = \pi/l$. This means that the order of the TC n may be determined by counting the flower's petals $n = 2\pi/\theta_0 = 2l$.

4. Results and Discussion

In accordance with the above experiment the order of TC has been received, so the sign of TC is let to measure. When the control signal of GCCD is resetting, the LG vortex beam reflected by M1 gets into the rectangular light path circulation with VPP by means of the transmission of GCCD. In the rectangular light path circulation, the LG vortex beam is in turn reflected by M2, M3 and M4. L1 and L2 are carried out on the LG vortex beam collimation. After the LG vortex beam is reflected even times, to be precise. Because the LG vortex beam is reflected a total of four times by M1, M2, M3, and M4, the TC sign of the LG vortex beam does not change as a result. When the LG vortex beam travels through the VPP. Following the second transmission of GCCD, the LG vortex beam is split in half with the assistance of BS1 in order to create two separate vortex beams. The next step in the process is the same as the one described before; however, for the purpose of clarity, we will not go into more detail. If the LG vortex beam goes through the VPP only once, the number of interference brilliant petals that occur between it and its conjugate beam will increase by two after the first time it does so. We are able to deduce from this whether the TC has a positive or negative value.

The interfering patterns for two beams with different experimental conditions, such as how the TCs are integers, fractions, and negative numbers are investigated experimentally and theoretically. The following will feature a one-by-one presentation of the outcomes.

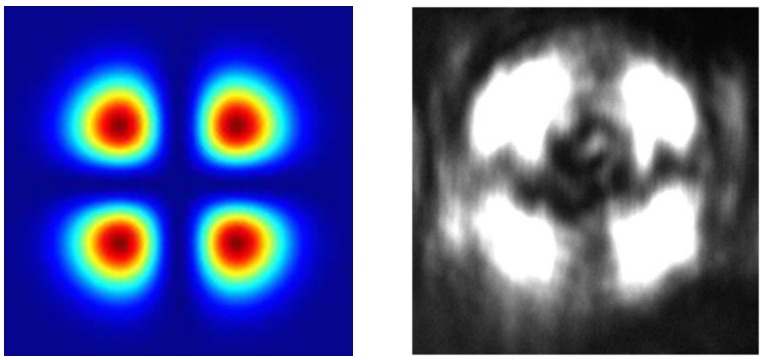

Figure 6. Theoretical and experimental interference patterns where (l=+2).

During the restoring of the GCCD signal, if $l = +2$ the frequency of petals in the CCD is 4, as shown in Figure 6. If $l = -3.5$ frequency of petals in the CCD represented in figure 7 is 5.

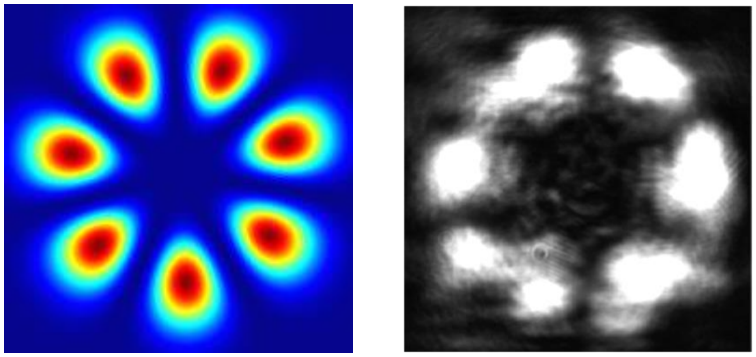

Figure 7. Theoretical and experimental interference patterns where ($l = -3.5$).

During the restoring of the GCCD signal, if $l = +2$ the frequency of petals in the CCD is 6, as shown in Figure 8. If $l = -3.5$ frequency of petals in the CCD represented in figure 9 is 5.

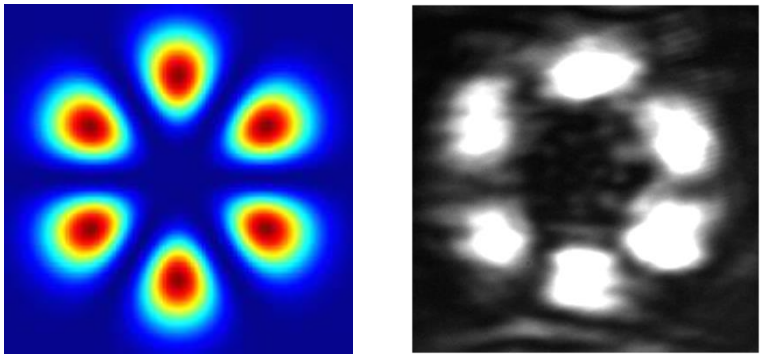

Figure 8. Theoretical and experimental interference patterns where ($l = +3$).

The suggested approach may be ridiculously simple without an influence of parasitic interference, that is induced by different devices along with the DP. Within that scenario, the sign of TCs is nevertheless empirically established, but even the order of TCs is also near to $l = 90$, which would be significantly more then employed in prior techniques.

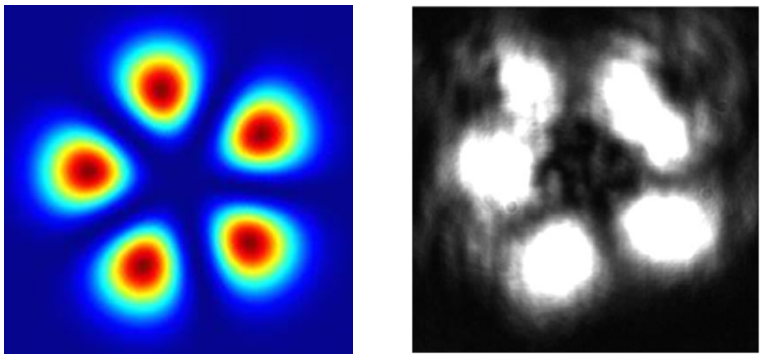

Figure 9. Theoretical and experimental interference patterns where ($l = -2.5$).

The optical system that we use in our technique is, on the other hand, very sensitive to the surrounding environment [45]. As a direct result of this, scientists with exceptional operating abilities and the ability to meticulously arrange the components of the experiment are necessary. Because the petals in our situation are not comparable to one another and do not constitute an integer, the given approach is not used in the process of evaluating other fractional-order TCs. Notwithstanding the limits of some test materials, like the CCD, the described approach may be used to detect the sequence and value of arithmetic and half-integer TCs, with the largest integer value being 90. This is made feasible by the demonstrated capability of the approach to measure the ordering of integer and half-integer TCs. In assessing comparatively small TCs in addition to higher-order TCs, research is still needed. Moreover, an investigation of LG vortex beams showed that the new strategy is effective. To apply the method that has previously proven effective in identifying the TCs of those other optical vortex beams, additional study is necessary.

5. Conclusion

Medical care system cannot be separated from comprehensive security protection and high-capacity information transmission, which can reduce medical risks and protect patient privacy. Quantum key distribution based on OAM can provide high security communication and large capacity information transmission for medical care system, among which the measurement of TCs of OAM is particularly critical. In a word, a new method based on interference intensity analysis is reported to identify and measure the order and the sign of integer and half-integer TCs of LG vortex beams. By counting the number of interference petal, and integer and half-integer TCs, we can be aware of the relationship of. If the LG vortex beam passes through the VPP for one time, then the number of interference bright fringes between the LG vortex beam and its conjugate beam increases by two, we can know that the sign of TC is positive and vice versa. And furthermore, the suggested method can be very plain but not vulnerable to the effect of parasitic interference, which is caused by some devices such as the DP. This technique can be used in a variety of applications, for instance optical communications, medical care, intelligent internet of vehicles, micro-particle manipulation, internet of things and so on.

Acknowledgements

This paper was supported partly by the National Natural Science Foundation of China under Grant 61871475, Special Project of Laboratory Construction of Guangzhou Innovation Platform Construction Plan under Grant 201905010006, Guangzhou Key Research and Development Project under Grant 202103000033, 201903010043, Guangdong Science and Technology Planning Project under Grant 2020A1414050060,2020B0202080002, 2016A020210122,2015A040405014, Innovation Team Project of Universities in Guangdong Province under Grant 2021KCXTD019, Characteristic Innovation Project of Universities in Guangdong Province under Grant KA190578826, Guangdong Province Enterprise Science and Technology Commissioner Project under Grant GDKTP2021004400, Meizhou City Science and Technology Planning Project under Grant 2021A0305010, Rural Science and Technology Correspondent Project of Zengcheng District, Guangzhou City under Grant 2021B42121631, Educational Science Planning Project of Guangdong Province under Grant 2020GXJK102, 2018GXJK072, Guangdong Province Graduate Education Innovation Program Project under Grant 2022XSLT056, 2022JGXM115.

References

[1] Donabedian A. 1966 Evaluating the quality of medical care[J] *The Milbank memorial fund quarterly* **44** (3) 166-206.
[2] Aday L A, Andersen R. 1974 A framework for the study of access to medical care[J] *Health Serv. Res* **9** (3) 208,.
[3] Rutstein D D, Berenberg W, Chalmers T C. Child 3rd C G, Fishman A P, Perrin E B, Evans C C. 1976 Measuring the quality of medical care: a clinical method. New Engl[J] *Med* **294** (11) 582-588.

[4] Arrow K J. 1978 Uncertainty and the welfare economics of medical care[J] *In Uncertainty in Economics* Academic Press 345-375.
[5] Greenfield S, Kaplan S H, Ware J E, Yano E M, Frank H J. 1988 Patients' participation in medical care[J] *J. Gen. Intern. Med.* **3** (5) 448-457.
[6] Green L A, Fryer Jr G E. Yawn B P, Lanier D, Dovey S M. 2001 The ecology of medical care revisited.
[7] McCaig L F, Burt C W. 2005 National hospital ambulatory medical care survey: 2003 emergency department summary *Adv data* **358** (1).
[8] Donabedian A. 2005 Evaluating the quality of medical care[J] *The Milbank Quarterly* **83** (4) 691-729.
[9] Cherry D K, Woodwell D A, Rechtsteiner E A. 2007 National ambulatory medical care survey: 2005 summary.
[10] Freidson E. 1974 Professional dominance: The social structure of medical care. Transaction Publishers.
[11] Starner T, Auxier J, Ashbrook D, Gandy M. 2000 The gesture pendant: A self-illuminating, wearable, infrared computer vision system for home automation control and medical monitoring. In Digest of Papers. *Fourth International Symposium on Wearable Computers* IEEE 87-94.
[12] Anliker U, Ward J A, Lukowicz P, Troster G, Dolveck F, Baer M, Belardinelli A. AMON: a wearable multiparameter medical monitoring and alert system. *IEEE T. Inf. Technol. B*. **8** (4) 415-427, 2004.
[13] Jurik A D, Weaver A C. Remote medical monitoring. Computer **41** (4) 96-99, 2008.
[14] Riurean S, Antipova T, Rocha Á, Leba M, Ionica A. 2019 VLC, OCC, IR and LiFi Reliable Optical Wireless Technologies to be Embedded in Medical Facilities and Medical Devices[J] *J. Med. Syst.* **43** (10) 308.
[15] Luff P. 2019 Emergency Medical Care in Chapter 74: Substantive Definitions and Interpretive Quandaries.
[16] Allen L, Beijersbergen M W, Spreeuw R J C, Woerdman J P. 1992 Orbital angular momentum of light and the transformation of Laguerre-Gaussian laser modes[J] *Phys. Rev. A.* **45** (11) 8185-8189.
[17] Zhang C, Guo B, Cheng G, Guo J, Fan R. 2014 Spin-orbit hybrid entanglement quantum key distribution scheme[J] *Sci. China-Phys. Mech. Astron* **57** (11) 2043-2048.
[18] Willner A E, Huang H, Yan Y, Ren Y, Ahmed N, Xie G, et al. 2015 Optical communications using orbital angular momentum beams[J] *Adv. Opt. Photonics* **7** (1) 66-106.
[19] Lei T, Zhang M, Li Y, Jia P, Liu G N, Xu X, et al. 2015 Massive individual orbital angular momentum channels for multiplexing enabled by dammann gratings[J] *Light-Sci. Appl*. **4** (3) e257.
[20] Ding D S, Zhang W, Zhou Z Y, Shi S, Xiang G Y, Wang X S, et al. 2015 Quantum storage of orbital angular momentum entanglement in an atomic ensemble[J] *Phys. Rev. Lett.* **114** (5) 050502.
[21] Shi C, Dubois M, Wang Y, Zhang X. 2017 High-speed acoustic communication by multiplexing orbital angular momentum. P. NATL. ACAD. SCI. USA. **114** (28) 7250-7253.
[22] Tamburini F, Thidé B, Molina-Terriza G, Anzolin G. 2011 Twisting of light around rotating black holes[J] *Nat. Phys* **7** (3) 195-197.
[23] Grier D G. 2003 A revolution in optical manipulation[J] *Nature* **424** (6950) 810-816.
[24] Zhou G Q, Cai Y J, Dai C Q. 2013 Hollow vortex Gaussian beams. Sci. China-Phys. Mech. Astron. **56** (5) 896-903.
[25] Chen M, Mazilu M, Arita Y, Wright E.M, Dholakia K. 2014 Optical trapping with a perfect vortex beam. //SPIE NanoScience+ Engineering, International Society for Optics and Photonics. 91640K-91640K-5.

[26] Guo J, Liang Y, Huang X G, Guo B, Li J. 2016 Pure dielectric waveguides enable compact, ultrabroadband wave plates[J] *IEEE Photonics J*. **8** (5) 1-9,.
[27] Liu A, Zou C L, Ren X, Wang Q, Guo G C. 2016 On-chip generation and control of the vortex beam[J] *Appl. Phys. Lett*. **108** (18) 181103.
[28] Guo J, Su W, Liang Y, Zhang F, Huang X. 2016 High-density information transmission and waveguide integration with low crosstalk and propagation loss[J] *Opt. Eng.* **55** (3) 037101.
[29] Cai K, Yang R, Li L, Ou S, Chen Y, Dou J. 2015 A semi-automatic coronary artery segmentation framework using mechanical simulation[J] *J. Med. Syst.* **39** (10) 129.
[30] Xiao B, Wang K, Bi X, Li W, Han J. 2018 2D-LBP: an enhanced local binary feature for texture image classification. IEEE T. Circ. Syst. Vid. 1-13. doi: 10.1109/TCSVT.2018.2869841.
[31] Chen H, Qiao H, Xu L, Feng Q, Cai K. 2019 A Fuzzy Optimization Strategy for the Implementation of RBF LSSVR Model in Vis-NIR Analysis of Pomelo Maturity. *IEEE T. Ind. Inform.* 1-9. doi:10.1109/TII.2019.2933582.
[32] Cai K, Yang R, Chen H, Li L, Zhou J, Ou S, Liu F. 2017 A framework combining window width-level adjustment and Gaussian filter-based multi-resolution for automatic whole heart segmentation[J] *Neurocomputing* 220 138-150.
[33] Leach J, Padgett M J, Barnett S M, Franke-Arnold S, Courtial J. 2002 Measuring the orbital angular momentum of a single photon[J] *Phys. Rev. Lett*. **88** (25) 257901.
[34] De Araujo L E, Anderson M E. 2011 Measuring vortex charge with a triangular aperture. *Opt. Lett.* **36** (6) 787-789.
[35] Vaity P, Banerji J, Singh R P. 2013 Measuring the topological charge of an optical vortex by using a tilted convex lens[J] *Phys. Lett. A.* **377** (15) 1154-1156,.
[36] Malik M, Mirhosseini M, Lavery M P, Leach J, Padgett M J, Boyd R W. 2014 Direct measurement of a 27-dimensional orbital-angular-momentum state vector[J] *Nat. Commun.* 5.
[37] Li X, Tai Y, Lv F, Nie Z. 2015 Measuring the fractional topological charge of LG beams by using interference intensity analysis[J] *Opt. Commun* 334 235-239.
[38] Emile O, Emile J, de Lesegno B V, Pruvost L, Brousseau C. 2015 Analysis of the topological charge of vortex beams using a hole wheel, EPL. 111, 34001.
[39] Lv F, Li X, Tai Y, Zhang L, Nie Z, Chen Q. 2015 High-order topological charges measurement of LG vortex beams with a modified Mach–Zehnder interferometer[J] *Optik*. **126** (23) 4378-4381.
[40] Guo J, Guo B, Fan R, Zhang W, Wang Y, Zhang L, Zhang P. 2016 Measuring topological charges of Laguerre–Gaussian vortex beams using two improved Mach–Zehnder interferometers[J] *Opt. Eng*. **55** (3) 035104.
[41] Zheng S, Wang J. 2017 Measuring orbital angular momentum (OAM) states of vortex beams with annular gratings[J] *Sci. Rep-UK*. 7 40781.
[42] Liu G G, Wang K, Lee Y H, Wang D, Li P P, Gou F, et al. 2018 Measurement of the topological charge and index of vortex vector optical fields with a space-variant half-wave plate[J] *Opt. Lett.* **43** (4) 823-826.
[43] Yin X, Hao J, Sang H, Han J, Xu C, Yang X, et al. China Patent. CN104007567A. 2014-08-27.
[44] Huang H, Xie G, Yan Y, Ahmed N, Ren Y, Yue Y, et al. 2014 100 Tbit/s free-space data link enabled by three-dimensional multiplexing of orbital angular momentum, polarization, and wavelength[J] *Opt. Lett* **39** (2) 197-200.
[45] Ke X Z, Chen J, Lv H. 2013 Effect of atmospheric turbulence on the orbital angular momentum of hollow vortex beams[J] *Sci. China Inf Sci*. **56** (12) 1-9.